

Improving an inkjet printer: saturation enhancement based on segmentation and hue*

Sige Hu¹, Baekdu Choi¹, George Chiu¹, Zillion Lin², Davi He², Jan Allebach¹

¹Purdue University, West Lafayette, IN 47906, U.S.A

²Sunvalley Tek, Shenzhen, China

Abstract

In one of our previous paper [1] proposed in the last year, we described the color management pipeline that applied to our nail inkjet printer. However, the resulting prints are not as vivid as we would like to have since those prints are not well saturated. In this paper, we propose a saturation enhancement method based on the image segmentation and hue angle. This method will not necessarily give us the closest representation of the colors within the input image but could give us more saturated prints. The main idea that we perform our saturation enhancement method is to keep the lightness and hue constant, while stretching the chroma component.

Introduction

To evaluate the quality of a print, color is one of the most important aspects to consider. Whether the color of the print is close to the original digital image or whether the color of print is well saturated are usually the factors that we consider to assess our own prints.

In a previous paper [1], we implemented a color management method in our printer, which includes tone correction, gamut mapping, and an inverse table method. The results of the prints do satisfy one of our criteria, which maps the output close to the original digital image. However, the gamut mapping procedure, which is used to compress the source gamut into the destination/printer gamut [1], results in less saturated prints. The low-saturation resulting prints are not as vivid as what we would like to have. Hence, we decided to develop a saturation enhancement algorithm, which could increase the chroma component while not shifting the hue value. Since the CMY color space is device-dependent and perceptually nonuniform, using the YyCxCz color space [2], which is both device-independent and more perceptually uniform, is expected to yield better results for saturation enhancement.

In this paper, we will introduce our saturation enhancement method in two sections. The first section is dedicated to illustrate the basic frame but also with its corresponding problems. The second section will mainly focus on two steps that we use to improve the deficiencies mentioned in the first section. This saturation enhancement method will be applied to the input image and then fed through our previously implemented color management pipeline [1].

Method

Basic framework

In this section, we will present our saturation enhancement algorithm basic framework. As we have emphasized, we would like to achieve our saturation enhancement in the YyCxCz color space due to its properties. Hence, given an input image, the first step is to perform sRGB to YyCxCz color space conversion for each pixel.

The second step is to stretch the chroma component while keeping the lightness and hue constant. This is our core idea to perform our saturation enhancement. But how are our YyCxCz components related to chroma, hue, and lightness? We use the following three equations in Eq. 1 - Eq. 2 as an illustration. According to the θ value in Eq. 1, we can calculate the hue angle which range from -180° to 180° according to the sector in $C_x - C_z$ plane. The hue angle actually represents the angle between the pixel location in $C_x - C_z$ plane and the C_x axis. We stretch the chroma as described in Eq. 3, where c_{new} is our new chroma value after stretching and c is the original chroma. c_{max} is the maximum chroma at the lightness and hue in the sRGB gamut that will be described in more details in the next section. γ is the power of stretching. We use Fig. 1 as an example to show the chroma stretched by three different γ values. As we can see from the plot, given the same input chrominance, the larger the γ value the larger the output chrominance.

After stretching the chroma, we finally apply our color management to the modified image, which maps the color into the printer gamut, as described in [1].

$$\theta = \left| \arctan(C_z/C_x) * \frac{180}{\pi} \right| \quad (1)$$

$$\text{Chroma} = \sqrt{C_x^2 + C_z^2} = c \quad \text{Lightness} = Y_y \quad (2)$$

$$c_{new} = c_{max} * f\left(\frac{c}{c_{max}}; \gamma\right) \quad (3)$$

$$f(x; \gamma) = 1 - (1 - x)^\gamma, \gamma > 1$$

Maximum chroma value c_{max} in sRGB gamut

To enable the basic framework to function, we need to know the maximum chroma of the sRGB gamut for each hue sector and lightness bin. We use Fig. 2 and Fig. 3 to illustrate how we obtain the maximum chroma value. Fig. 2 is the top view

*Research supported by Sunvalley Tek, Shenzhen, CHINA.

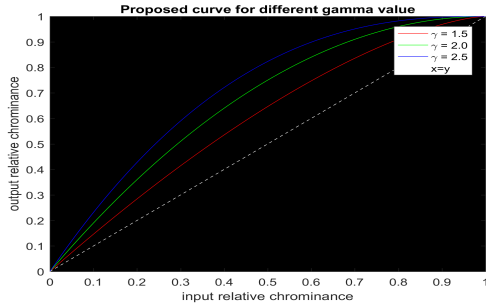


Figure 1. Proposed chroma stretching curve.

of our gamut in $Y_y C_x C_z$ color space where we project our whole gamut onto the $C_x - C_z$ plane. We define the origin point to be $(C_x, C_z) = (0, 0)$, and we simply divide the gamut into 72 hue sectors with each sector corresponding to 5 degrees starting from 0. The small blue region in Fig. 2 is one example hue sector for hue angle between 60 and 65 degrees. If we inspect our example hue sector between 60 and 65 degrees in a side view, we obtain the plot shown in Fig. 3, where the x-axis represents the chroma value and y-axis represents lightness/ Y_y value. Since Y_y ranges from -16 to 100, we simply divide it into 116 Y_y bins and assume that within each bin the maximum chroma is a constant. Therefore, the C_{max} value of the sRGB gamut can be stored into a two dimension array $C_{max}[72][116]$, and the specific C_{max} value of each pixel can then be acquired by a given corresponding hue sector and Y_y bin number.

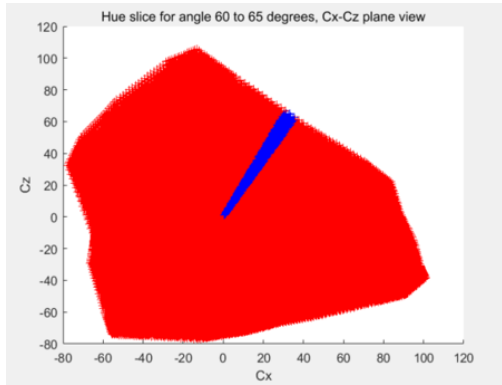


Figure 2. Top view of gamut (projection to $C_x C_z$ plane).

Result analysis

Basic framework method analysis

After applying our first stretching curve based on Eq. 3 with $\gamma = 2.5$, we obtain our first saturation enhancement test result, which is shown in Fig. 4. The right image shows an obvious increase in color saturation for the apple. It results in a brighter red apple compared to the left original image, which makes the colors more vivid. Meanwhile, since we only stretch the chroma value and keep the hue unchanged, the saturated color will not shift to another strange color. We could fine-tune the γ value to acquire more visually pleasant results if this method worked well for all test images. However, this first proposed method for saturation enhancement has two problems. The first one is that some neutral

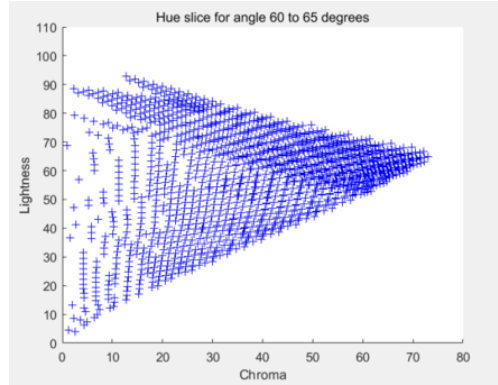


Figure 3. Hue sector side view for the hue sector shown in Fig. 2.

colors become visibly non-neutral; and the second one is that human faces (flesh tone) colors tend to become too yellow. We will briefly describe each problem and our proposed solution to it in the next two sections.

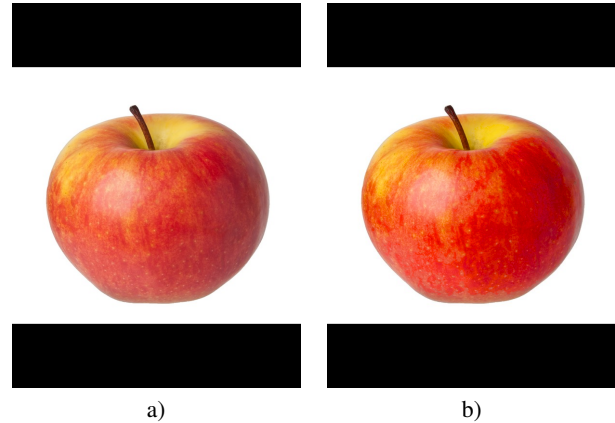


Figure 4. Comparison between the original input image and the first saturation enhancement result: a) Original input image. b) Saturation enhancement result.

Neutral color problem and solution

The first problem is correlated to neutral colors such as black and white. In Fig. 5, we notice that after saturation enhancement the white background becomes slightly yellowish and the black suit tends to be blueish. People might not consider this to be a serious problem since the color is still light but this could cause very visible noise for a print with a white background. This is especially true for our nail printer, for which we need to apply a pure white nail gel at the preparation stage. Hence, we propose a method, which could keep our neutral colors to be neutral.

To solve this neutral color problem, we decide to modify the stretching function, which we apply to enhance the chroma value, so that when the input chroma is below a certain threshold, the chroma is not changed. We come up with this idea because the neutral color always corresponds to a small chroma value. Hence, if we set a threshold to the input chroma, we can filter out the low chroma-value neutral colors without stretching them. Equation 4, which is a modification of the second line of Eq. 3 illustrates our solution and the plots in Fig. 6 show the comparison between the

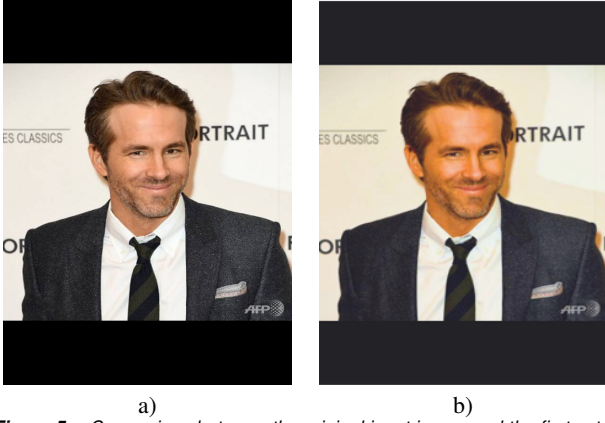


Figure 5. Comparison between the original input image and the first saturation enhancement result (Eq. 3 line 2) with $\gamma = 2.5$: a) Original input image. b) Saturation enhancement result.

original stretching curve and the new threshold applied stretching curve. We define a threshold t in the new function, which keeps the chroma unchanged when the chroma is smaller than this threshold, and perform the γ stretching only if the chroma value is larger than the threshold. We consider several test images to narrow down the threshold value and we find out the threshold value between 0.2 and 0.25 give us the most reasonable results even though this decision is slightly subjective. In Fig. 6, we represent the newly proposed stretching curve compared to our original stretching curve with threshold $t = 0.2$. The new stretching curve above the threshold is basically the squeezed and shifted form of our original curve.

$$f(x; \gamma, t) = \begin{cases} x, & \text{if } x < t \\ t + (1-t) \left[1 - \left(1 - \frac{1}{1-t} (x-t) \right)^\gamma \right] & \text{if } x \geq t \end{cases} \quad (4)$$

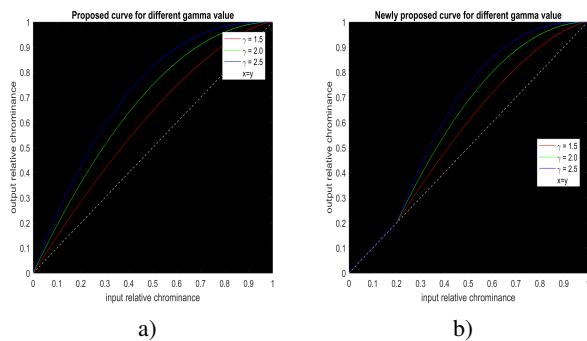


Figure 6. Comparison between the stretching curve: a) Original proposed stretching curve. b) Newly proposed stretching curve with threshold $t = 0.2$.

To compare the saturation enhancement result of the original stretching and the new stretching that is shown in Fig. 7, we should focus mostly on two parts - the white background and the black suit. The right image, which is the new saturation enhanced result, is obviously more neutral on those two parts compared to the original stretched image shown on the left. Hence, setting a threshold value to activate the stretching curve does help us to keep the neutral colors neutral.

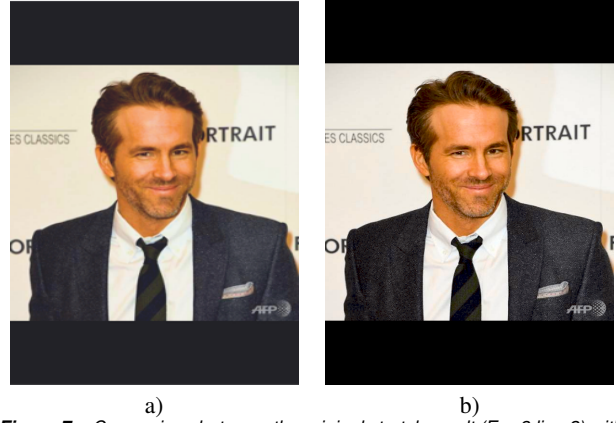


Figure 7. Comparison between the original stretch result (Eq. 3 line 2) with $\gamma = 2.5$ and the newly proposed stretch result (Eq. 4) with $\gamma = 2.5$ and $t = 0.2$: a) Original stretch. b) Newly proposed stretch.

Flesh tone colors mapping problem and solution

Problem and investigation

The second problem we find in our original proposed stretching is that the flesh tone colors tend to become too yellow. This could not be solved by simply setting a threshold value. What we come up with first is to find which hue sectors are likely to contain human face colors (flesh tone colors), and we can make smaller changes for colors in those hue sectors. The basic idea is to segment the input image into two parts according to their hue values and apply the same stretch function, but with two different γ values. Hence, the hue range related to the flesh tone colors will have less change and the color would be closer to original image.

To address the human face mapping issue, we first investigate the hue values of different human faces, including different type skin colors. We use Fig. 8 as an example to illustrates our investigation. The left pie circle is a $C_x - C_z$ plane diagram and the angle between the current pixel position in $C_x - C_z$ plane; and the C_x axis is the hue angle, which varies from -180 to 180 degrees. For each human face, we randomly pick several pixel points and record their hue values. On the right human face image in Fig. 8, we randomly pick two points and locate their $C_x - C_z$ values on the left pie. In this example, we only pick two sample points to make this illustration more concise; but we pick many more points in the real investigation to reduce randomness. For our example in Fig. 8, the hue values of these two sample points are 44.92° and 45.34° based on Eq. 1, and we can observe that the color around 45° on the left pie diagram is similar to the color of these two sample points. Once we collect all the hue values from different sample points from different human face images, we can then determine the hue range corresponding to the flesh tone colors and apply a smaller change to this hue range.

Hue dependent saturation enhancement

Based on our investigation of flesh tone colors, we find that the flesh tone colors are mostly in the hue range 20° to 70° . Hence, we apply a smaller gamma stretching inside this hue range. According to several experiments with different combinations of γ values, we find that assigning $\gamma = 1.2$ to this hue range for flesh tone colors and $\gamma = 2.5$ to all other hue values gives us the best result. Except for applying different γ values, these two

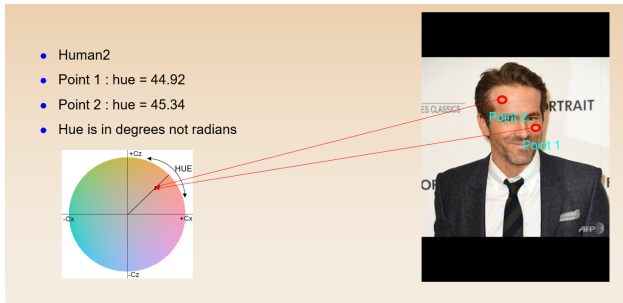


Figure 8. Example of flesh tone color investigation.

parts both stretch the chroma value by using Eq. 4.

Comparison of the original saturation enhancement and hue dependent saturation enhancement result is shown in Fig. 9. The bottom right image c) is our hue dependent saturation enhancement result; and we can clearly see that the flesh tone/face color is much closer to the original image shown in the Fig. 9 top image a).



Figure 9. Comparison between the original saturation enhancement result and the newly proposed hue dependent saturation enhancement result.

The comparison in Fig. 9 indicates that our method to apply a smaller γ stretching to flesh tone colors helps us solve the over saturation enhancement issue. However, the hue range with fixed values results in a boundary discontinuity issue, which is shown in Fig. 10. The left bread image is our hue dependent sat-

uration enhancement result and the right image is the zoom-in of the red circle region on the left image. By concentrating on the right image, we observe that the color on the cut bread surface is not smooth, since some pixels are dark yellow while some other pixels are bright yellow. To confirm the cause of this discontinuity, we choose two pixels which have very different yellow appearance after saturation enhancement, and find that their chroma values before saturation enhancement are very similar. However, their hue angles are located on the two sides of the boundary hue angle 70° , which are around 69° and 73° . These close hue angles located next to the boundary hue value but on different sides of it result in two different γ value stretches, thus leading to two dissimilar output chroma values.

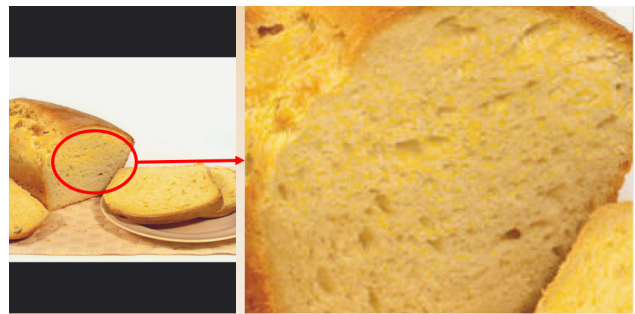


Figure 10. Fixed hue range hue dependent saturation enhancement result illustrating discontinuities at the hue boundaries.

Saturation enhancement by different gamma values – based on image-dependent hue range

To solve this discontinuity issue, we decide to figure out a way to make the hue range more flexible, which is image-dependent instead of using the fixed numbers $[20^\circ, 70^\circ]$ as the range. We first attempt to achieve this goal by using a connected components method but find that it performs poorly in some specific texture regions. After some discussions, we realize that the method mentioned in [3] could help us to determine the flexible flesh tone hue range.

This new approach mainly consists of three steps. We first follow the method in [3] to obtain a merge image with a given number of clusters. The basic idea behind this is image segmentation. Secondly, we find the hue range of each cluster. Finally, among these clusters, we choose that one with hue range closest to the fixed hue range $[20^\circ, 70^\circ]$ and apply a smaller gamma value within this range. This new approach inherits the idea of the hue-dependent method, while varying the hue range image-dependently to handle the boundary artifacts.

We follow the method in [3] to obtain the merge image by combining a K-means cluster map and a segmented edge map. The K-means cluster map is generated follow the standard naive K-means algorithm [8]. The idea behind using the edge map is to avoid changing the γ value within a smooth region, where a chroma change artifact would be most noticeable. To generate the segmented edge map, we first convert the color space from sRGB to CIE La^*b^* and apply a bilateral filter, which is used to smooth the input image. The bilateral filter is a 3 by 3 filter with $\sigma_s = 21.63$ and $\sigma_r = 2$, where σ_s is the standard deviation of spatial smoothing; and σ_r indicates the range of tolerance

in color difference. Increasing the spatial parameter σ_s smooths larger features, and as the range parameter σ_r increases, the bilateral filter gradually approximates Gaussian convolution more closely. Then, we use the Sobel edge detector mentioned in [3], [4], followed by the hysteresis threshold [5] that improves the performance compared to a simple threshold. We apply the algorithm in [6] to thin the edge map, and finally acquire the segmented image by connected components and sorting. We sort the connected components in descending order of segment size; and we merge all small segments to keep the number of segments to a predefined number S , which in our case is 64. To merge the K-mean cluster map and the segmented edge map, we count the pixels that have the maximum cluster number within each segment, and assign this maximum cluster number to the whole segment. In addition to the steps in [3], we also try to implement an edge linking algorithm [7] to achieve a better edge map. However, this method costs much more time, while the result does not exhibit much difference. So we finally decide not to add the step of edge linking. The block diagram of the whole procedure is shown in Fig. 11; and an example of the result of the segmented edge map, the K-means cluster map and the merge map is shown in Fig. 12.

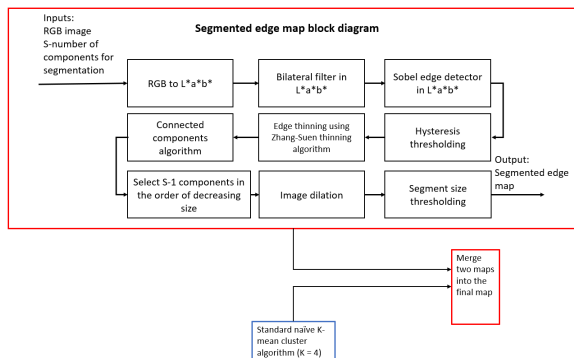


Figure 11. The block diagram to generate the final merge map.

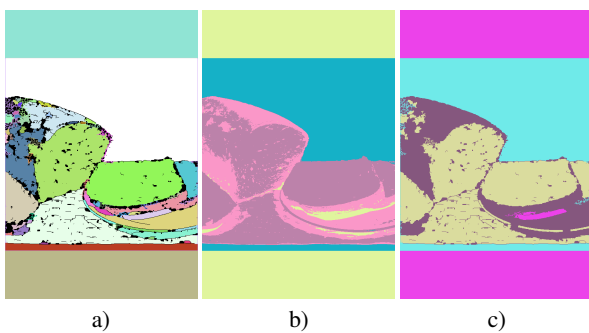


Figure 12. a) Sorted segment image. b) K-means cluster image c) Merge map.

We consider that the noise pixels on the cut bread surfaces might still affect the result of our hue range selection. Hence, we decide to apply image morphology [9] and a segment size threshold. Image morphology is a technique to remove the noise pixels in the binary image by accounting for the form and structure of the image. There are two basic image morphology operations, which are image dilation and image erosion; and by combining these two basic operations, there are also image closing and image

opening. We find that image dilation performs the best to remove noise pixels; and the result is shown in Fig. 13. By comparing to the original sorted image in Fig. 12, this new sorted image after the image morphology operation has many fewer noise pixels. To remove the leftover small segments, we merge all small segments into surrounding large segments by thresholding the segment size. Then we merge the segment image and the K-means image into our final merge map as shown in the Fig. 13 right image.

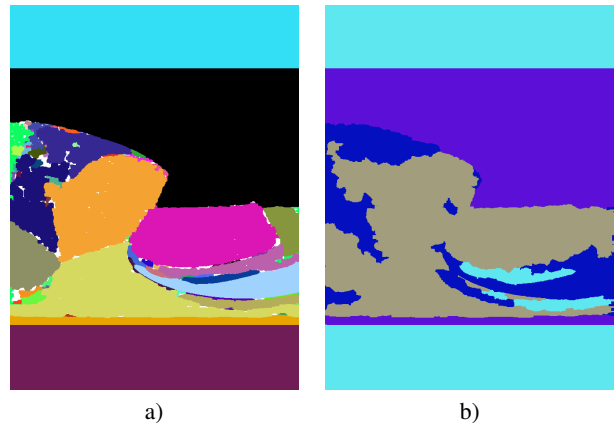


Figure 13. a) Sorted segment image after image morphology. b) Final merge map.

After we obtain our merge map, we then acquire the hue range in each segment and find the hue range closest to hue range $[20^\circ, 70^\circ]$. The final saturation enhancement result is compared to the result of saturation enhancement with a fixed hue range in Fig. 14. The right image in Fig. 14 is our image-dependent hue range result, which is much smoother compared to the left fixed hue range result. By comparing more test images, we conclude that our image-dependent hue range saturation enhancement method does solve the boundary issue of discontinuities.

After solving the neutral color and discontinuity problems, we want to know how does our final saturation enhancement algorithm perform. Hence, we experiment with several test images and one attractive result is shown in Fig. 15. The left image is the original image and the right one is our final saturation enhancement result. As we can see, the background grass is shown in a much brighter color and the back area of the deer tends to be more brown, which results in a more vivid result. Meanwhile, by focusing on the bottom text region, we notice that the neutral color with small chroma value is not affected, as we expect. Figure 16 shows some additional results, including images of two individuals with darker skin tones. It can be seen that the flesh tones are preserved, and the saturation of other colors is generally enhanced.

Conclusion

In this paper, we introduce a saturation enhancement algorithm by keeping the lightness and hue as constant while stretching the chroma component. Our final results improve the vividness and help us to increase the saturation of images. We introduce three main developments compared to the basic framework for saturation enhancement. To keep neutral colors neutral, we apply a threshold to the normalized chroma value. To alleviate the excess saturation for flesh tone colors, we apply a smaller saturation power (smaller gamma value) to the hue range of flesh tone

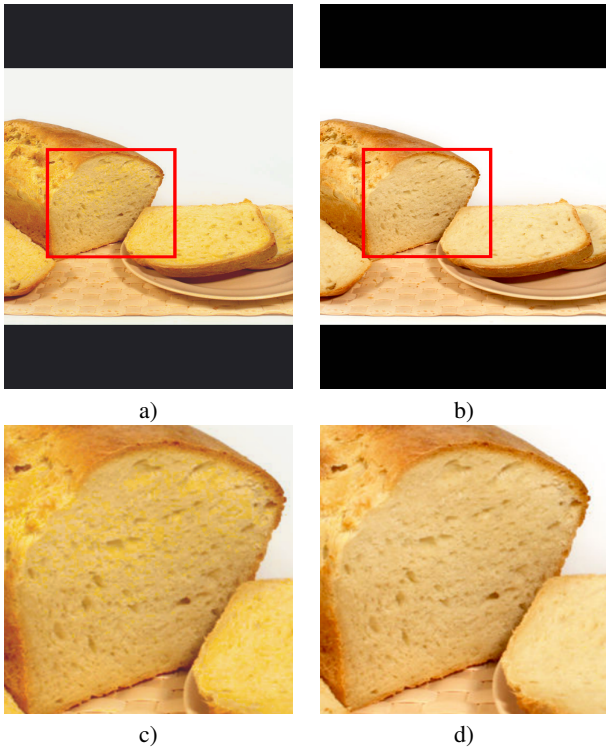


Figure 14. a) Fixed hue range saturation enhancement result. b) Image-dependent hue range saturation enhancement result. c) Zoom-in of the red rectangle region on the image a). d) Zoom-in of the red rectangle region on the image b).

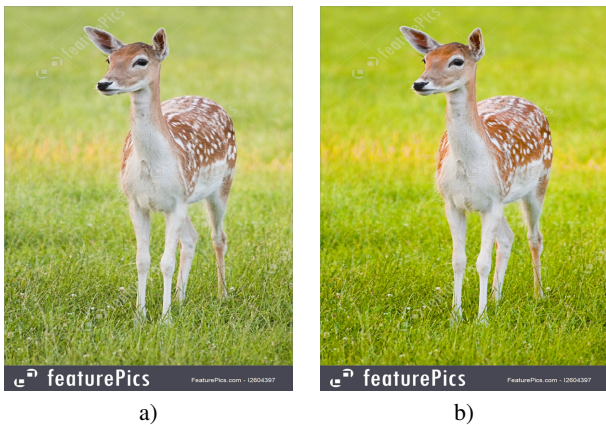


Figure 15. a) Original image. b) Final saturation enhancement result.

colors. And in order to solve the discontinuity problem, we set the hue range of flesh tone colors in an image-dependent manner, according to segmentation of the image. However, there are still some aspects we can improve in the future. First, our K-means clustering algorithm currently using a fixed number of four clusters. This could be improved by allowing a flexible number of cluster that is image-dependent. Furthermore, we can find a more precise method to choose the hue range since there are still some test images that fail to find a reasonable hue range, which result in the default hue range.

References

- [1] Wang, Yin, et al. "Developing an inkjet printer I: RGB image to CMY ink amounts-Image processing and color management." *Electronic Imaging 2020.15* (2020): 350-1.
- [2] Flohr, Thomas J., et al. "Model-based color image quantization." *Human Vision, Visual Processing, and Digital Display IV*. Vol. 1913. International Society for Optics and Photonics, 1993.
- [3] Jumabayeva, Altyngul, et al. "Content-color-dependent screening (CCDS) using regular or irregular clustered-dot halftones." *2018 7th European Workshop on Visual Information Processing (EUVIP)*. IEEE, 2018.
- [4] Seger, Olle. "Generalized and separable sobel operators." *Machine Vision For Three-Dimensional Scenes* (2012): 347.
- [5] Canny, John. "A computational approach to edge detection." *IEEE Transactions on Pattern Analysis And Machine Intelligence* 6 (1986): 679-698.
- [6] Zhang, T. Y., and Ching Y. Suen. "A fast parallel algorithm for thinning digital patterns." *Communications of the ACM* 27.3 (1984): 236-239.
- [7] Akinlar, Cuneyt, and Edward Chome. "PEL: a predictive edge linking algorithm." *Journal of Visual Communication and Image Representation* 36 (2016): 159-171.
- [8] MacQueen, James. "Some methods for classification and analysis of multivariate observations." *Proceedings of the Fifth Berkeley Symposium on Mathematical Statistics And Probability*. Vol. 1. No. 14. 1967.
- [9] Haralick, Robert M., Stanley R. Sternberg, and Xinhua Zhuang. "Image analysis using mathematical morphology." *IEEE Transactions on Pattern Analysis And Machine Intelligence* 4 (1987): 532-550.

Author Biography

Sige Hu received his BS in Electrical and Computer Engineering from Pennsylvania State University (2017) and is currently pursuing PhD in Electrical and Computer Engineering at Purdue University. His research is mainly focus on image processing.

Baekdu Choi received his B.Sc. in electrical and computer engineering from Seoul National University, Seoul, South Korea in 2017 and is currently working on a Ph.D. in electrical and computer engineering at Purdue University, West Lafayette, IN, USA. His research mainly focuses on digital image processing, digital halftoning and color management for inkjet printers.

George T. Chiu is a Professor in the School of Mechanical Engineering with courtesy appointments in the School of Electrical and Computer Engineering and the Department of Psychological Sciences at Purdue University. He also serves as the Assistant Dean for Global Engineering Programs and Partnership for the College of Engineering. Dr. Chiu received the B.S. degree in Mechanical Engineering from the National Taiwan University in 1985 and the M.S. and Ph.D. degrees in Mechanical Engineering from the University of California at Berkeley, in 1990 and 1994, respectively. From September 2011 to June 2014, he served as the Program Director for the Control Systems Program at the National Science Foundation. His current research interests are mechatronics and dynamic systems and control with applications to digital printing and imaging systems, digital fabrications and functional printing, human motor control, motion and vibration perception and control. He received the 2012 NSF Director's Collaboration Award and the 2010 IEEE Transactions on Control System Technology Outstanding Paper Award. He served as the Editor-in-Chief for the IEEE/ASME Transactions on Mechatronics from 2017-19 and as the Editor for the Journal of Imaging Science and

Technology from 2012-14. Dr. Chiu served on the Executive Committee of the ASME Dynamic Systems and Control Division (DSCD) from 2007 to 2014 and as the Chair of the Division from 2012-13. He is a Fellow of ASME and a Fellow of the Society for Imaging Science and Technology (IS&T).

Peng (Davi) He is a software manager in Sunvalleytek International Inc, Shenzhen, Guangdong, China. He received his B.S in Communication Engineering from Hunan University of Arts and Science, Changde, Hunan, China in 2012.

Zillion (Zhenqing) Lin is a technical director in Sunvalleytek International Inc, Shenzhen, Guangdong, China. He received his BS in Microelectronics Engineering from University of Electronic Science and Technology of China, Chengdu, Sichuan, China in 2008 and MS in Biomedical Engineering from Shenzhen University, Shenzhen, Guangdong, China. His current research interest including artificial intelligence and robot.

Jan P. Allebach is Hewlett-Packard Distinguished Professor of Electrical and Computer Engineering at Purdue University. Allebach is a Fellow of the IEEE, the National Academy of Inventors, the Society for Imaging Science and Technology (IS&T), and SPIE. He was named Electronic Imaging Scientist of the Year by IS&T and SPIE, and was named Honorary Member of IS&T, the highest award that IS&T bestows. He has received the IEEE Daniel E. Noble Award, the IS&T/OSA Edwin Land Medal, the IS&T Johann Gutenberg Prize, and is a member of the National Academy of Engineering

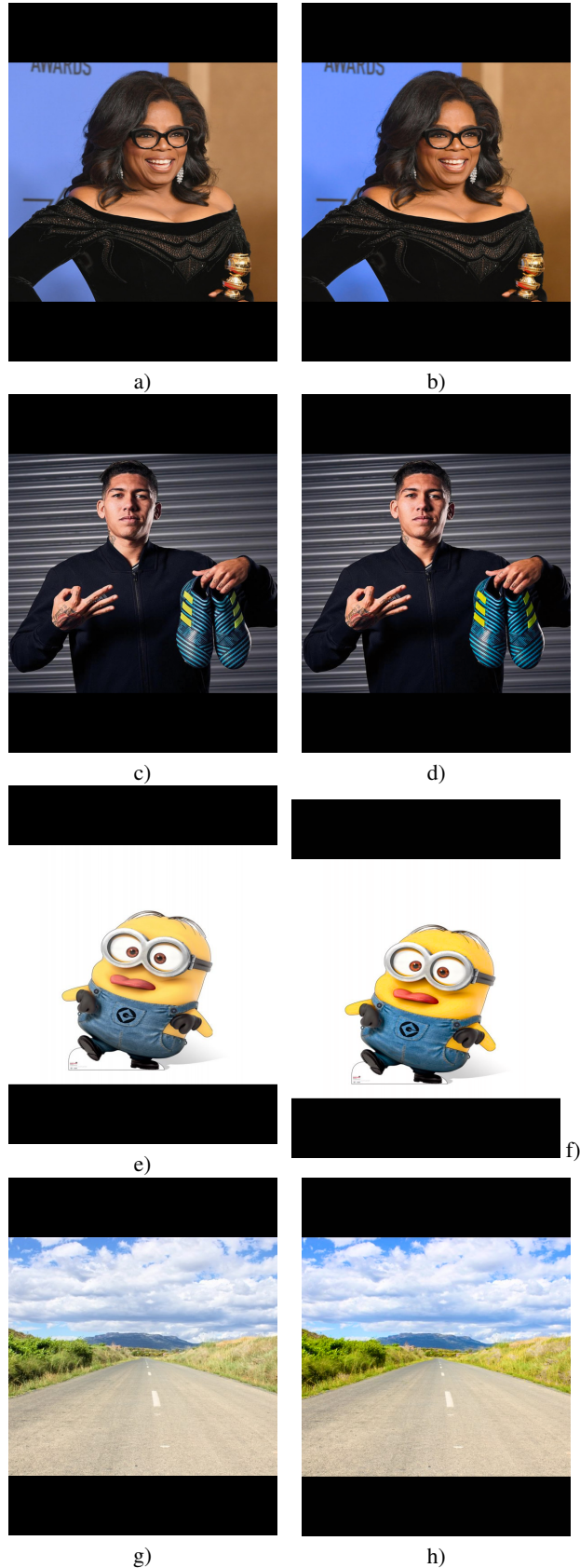


Figure 16. a), c), e), g) (left) Original images. b), d), f), h) (right) Final saturation enhancement result.

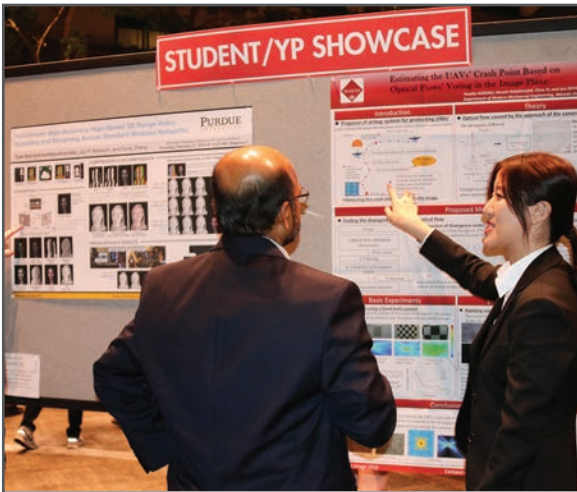
JOIN US AT THE NEXT EI!

IS&T International Symposium on

Electronic Imaging

SCIENCE AND TECHNOLOGY

Imaging across applications . . . Where industry and academia meet!



- **SHORT COURSES • EXHIBITS • DEMONSTRATION SESSION • PLENARY TALKS •**
- **INTERACTIVE PAPER SESSION • SPECIAL EVENTS • TECHNICAL SESSIONS •**

www.electronicimaging.org

